crystals

MDPI

Article

Enhancing Photoluminescence and Stability of $CsPbI_3$ Perovskite Quantum Dots via Cysteine Post-Processing

Sijie Chen, Jianwu Wei and Qi Pang *

School of Chemistry and Chemical Engineering/Guangxi Key Laboratory of Electrochemical Energy Materials, Guangxi University, Nanning 530004, China
* Correspondence: pqigx@163.com

Abstract: Red-emitting cesium lead iodide ($CsPbI_3$) perovskite quantum dots (CQDs) are extremely unstable due to their structural composition and the weak binding force of ligands on the surface of nanocrystals. Herein, we report an effective method to enhance the photoluminescence and stability of CQDs by simple post-processing with cysteine (Cys). Compared to the pristine CQDs with a photoluminescence quantum yield (PLQY) of 38.61%, the Cys-processed one has fewer surface defects, obtaining a PLQY of 70.77%, nearly twice as much as the pristine samples, and, simultaneously, the Cys-processed CQDs retained more than 86% of the initial PL intensity after 20 days of storage in the atmosphere. This research provides a new idea for the preparation of high-performance and red-emitting quantum dots.

Keywords: $CsPbI_3$; quantum dots; post-processing; stability; cysteine

check for updates

Citation: Chen, S.; Wei, J.; Pang, Q. Enhancing Photoluminescence and Stability of $CsPbI_3$ Perovskite Quantum Dots via Cysteine Post-Processing. *Crystals* **2023**, *13*, 45. https://doi.org/10.3390/cryst13010045

Academic Editor: Maria Gazda

Received: 30 November 2022
Revised: 21 December 2022
Accepted: 22 December 2022
Published: 27 December 2022

Copyright: © 2022 by the authors. Licensee MDPI, Basel, Switzerland. This article is an open access article distributed under the terms and conditions of the Creative Commons Attribution (CC BY) license (https://creativecommons.org/licenses/by/4.0/).

1. Introduction

Lead halide perovskites have aroused great interest over the years due to their outstanding optical-electrical properties, such as high photoluminescence quantum yield (PLQY), narrow full-width at half-maximum, and tunable band gap [1–3]. Cesium lead iodide ($CsPbI_3$) perovskite quantum dots (CQDs) have the lowest band gap with 1.80 eV [4], which is particularly suitable for manufacturing solar cells and red-light-emitting diodes [5–9]. However, the CQDs can easily lose their structural integrity under light or humidity, leading to degradation or unwanted phase transition from the black cubic phase to the yellow orthorhombic phase with poor photoelectric properties at room temperature [10–13]. Although long-chain organic ligands such as oleic acid (OA) and oleyamine (OAm) are usually used to surface treat and stabilize the CQDs, they are easily detached from the surface of CQDs during the purification process because of the poor binding force between the ligands and the surface ions [14,15]. The ligand loss increases the surface defects of the perovskites, which not only induces detrimental non-radiative recombination paths but also accelerates the phase transition, seriously limiting its application and development [16,17].

To address these issues, great efforts have been devoted to obtaining high-performance and highly stable CQDs. Some of them improve the stability of the optically active phase by in situ mixing the ABX_3 crystal structure of perovskite. For instance, doping $CsPbI_3$ with other smaller metal cations such as Ca^{2+}, Sr^{2+}, Mn^{2+}, and Sn^{2+} at B-sites to directly regulate the internal lattice structure is an effective method to significantly adjust the lattice distortion of the cubic $CsPbI_3$, effectively improving the stability of the perovskites [18–22]. It is the same for the partial substitution of cesium cations by other A-site cations such as methylamine or formamidine and partial substitution of iodine ions by bromine or chlorine [23–25]. In parallel, treating the X-site vacancies on the surface of the cubic $CsPbI_3$ perovskites by adding SCN^- and I^- anions indirectly affects lattice symmetry, treats the available surface defects, and significantly enhances the stability of the cubic $CsPbI_3$ perovskites [26,27]. Yao et al., reported a novel strontium substitution, along with

an iodide suppression strategy, to synthesize the cubic CQDs with high stability and high luminescence performance, achieving the facile synthesis of the cubic CQDs with a series of controllable sizes down to below 5 nm [28]. Lu et al. also reported a method achieving highly luminescent and robust cubic CQDs through engineering the lattice symmetry of perovskite, which was enabled by the synergistic effect of Cl^- ion suppression and Sr^{2+} ion doping [29]. However, while in situ ion substitution is effective in suppressing defects, the introduction of other metal ions may affect the emission position. Meanwhile, the presence of long-chain insulating ligands on the surface remains, affecting the carrier transport to hinder device development.

To overcome this problem, processing the surface of the synthesized CQDs with other ligands is a viable method. In recent years, ligand exchange has been widely used to treat the surface defects of the perovskites [30–32]. Huynh et al. used sulfur-OAm to passivate the defective surface of CQDs. Compared with OAm, sulfur in sulfur-OAm can provide a more powerful suppression effect to prepare stable CQDs [33]. Tian et al. reported a method exchanging the original long-chain ligands with 2-aminoethanethiol (AET) to obtain highly stable CQDs [34]. This provides us with a hint that other special functional groups, in addition to carboxyl and amino groups, seem to provide more efficient suppression. Zhang et al., showed that the CQDs modified with C8 ligands (such as caprylic acid and octyl amine) have stronger binding energy, better stability, and higher quantum yield than those modified with C18 ligands (such as oleic acid and oleamine) [16]. Replacing partial long-chain ligands with short-chain ligands can notably enhance the binding ability of surface ligands to the surface ions of perovskites, thus improving the stability of the cubic CQDs. Based on this, we believe that it is a promising approach to find short-chain ligands with special functional groups to process the surface of CQDs for high performance and high stability.

Amino acids are common amphoteric substances, and their carboxyl and amino groups make it possible for them to simultaneously replace OA and OAm on the surface of CQDs. Meanwhile, their short-chain molecular structure enables them to easily overcome the steric hindrance of OA and OAm and effectively process surface defects of CQDs, and a series of amino acids were proved to be effective in optimizing CQDs [35,36]. Short-chain cysteine (Cys) not only retains the amino acid's signature amphoteric functional groups (carboxyl and amino) but also has thioxo. It has been proven to be effective in processing surface defects in CdSe QDs [37–40]. The three-functional group structure of Cys can bring a more excellent coordination effect, and the short-chain molecular structure makes it easier to overcome the steric hindrance of OA and OAm.

In this scenario, the Cys was used as a tridentate ligand for the post-processing of CQDs with a strategy for substitution of parts OA and OAm, meanwhile maintaining the cubic phases of the perovskites. A time-resolved photoluminescence (TRPL) study revealed a much longer photoexcited exciton lifetime in the Cys-processed CQDs than the pristine CQDs, which points to a significant reduction in the quenching defects, demonstrating that Cys can effectively suppress the surface defects of CQDs and maintain the cubic phases. Our findings thus lay the foundation for manufacturing photoelectric materials with high stability and efficiency.

2. Materials and Methods

2.1. Materials

Cs_2CO_3 (99.9%), PbI_2 (99.9%), Octadecene (ODE, 90%), oleic acid (OA, 90%), oleylamine (OAm, 90%), cysteine (Cys, 99%), Ethyl acetate (EtOAc, 99%), and hexane (95%) were purchased from Macklin and all were used directly.

2.2. Preparation of Cs-Oleate

Synthesis of Cs-Oleate

Cs_2CO_3 (0.25 g) was loaded into 50 mL 3-neck flask along with ODE (25 mL) and OA (1 mL), degassed under vacuum for 1 h at 120 °C, and then heated under N_2 to 150 °C

until all Cs_2CO_3 reacted with OA. Since Cs-oleate can precipitate out of ODE solution at room-temperature, it has to be preheated to 120 °C before injection.

2.3. Synthesis of CQDs

PbI_2 (0.3 g), OA (1.5 mL), OAm (1.5 mL), and ODE (15 mL) were mixed into 50 mL 3-neck flask with stirring and degassed under vacuum at 120 °C for 1 h. After complete solubilization of PbI_2, the flask was connected to N_2 protection and the temperature was raised to 150 °C, and 2.4 mL of Cs-oleate solution was swiftly injected into the above hot mixture and the reaction was stopped with an ice-water bath after 5 s. The crude products were centrifuged at 8000 rpm for 10 min. Then the supernatant was discarded and the precipitate was redispersed in hexane for further treatment.

Post-Processing of CQDs

The post-processing solutions were prepared by dissolving the Cys into the solution of EtOAc, and then the CQDs were added into the ligand solutions. After dissolving by ultraphonic treatment for a few minutes, the mixed solutions were centrifuged at 8000 rpm for 5 min. Then, the supernatants were discarded and the precipitates were collected and dispersed in 5 mL hexane for the next measurements.

3. Characterizations

The phase identification was carried out using powder X-ray diffraction (XRD, DX-2700A, DanDong, China). The morphology and crystal structure of the prepared CQDs were characterized using a transmission electron microscopy (TEM, FEI TECNAI G2 F30, Portland, American). The UV−vis absorption spectra were measured using a spectrophotometer (UV, UV-1700, Kyoto, Japan). The Fluorescence emission spectra was recorded on an FLS1000 spectrophotometer (PL, Edinburgh Instrument, Edinburgh, the United Kingdom). The fluorescence lifetimes of the synthesized $CsPbI_3$ perovskite QDs were recorded by using a time-resolved single-photon-counting spectroflfluorometer (TRPL, λex = 405.2 nm, FLS1000, Edinburgh Instrument, Edinburgh, UK). The absolute fluorescence quantum yield of the QD solutions was measured by using an integrating sphere on an Absolute PL quantum yield spectrometer (PLQY, FLS1000, Edinburgh Instrument, Edinburgh, UK). The binding energies and valence states of elements were measured by X-ray photoelectron spectroscopy using the Thermo Fisher ESCALAB Xi with 14.6 kV working voltage and AlKα rays for the excitation source (XPS, Waltham, MA, USA). The Fourier transform infrared spectra were measured on a Fourier infrared spectrometer (FTIR, Nicolet iS 50, Waltham, MA, USA).

4. Results and Discussion

The CQDs were generally capped by oleic acid and oleamine and synthesized using a previously reported hot-injection method with several modifications [4], and Cys was introduced for post-processing on the CQDs surface, which was prepared by dispersing in ethyl acetate (EtOAc) to a range of concentrations of 0.025, 0.050, 0.075, and 0.100 M for post-processing; this post-processing as well as the storage of samples was carried out in an atmosphere with an average temperature of 30 °C and an average humidity of 85%.

Figure 1a is the XRD patterns of the pristine CQDs and the Cys-processed CQDs. The peaks were around 14° and 28°, which is in good agreement with the (100) and (200) planes of the $CsPbI_3$ cubic phase [33]. This indicates that the processing of the CQDs surface by Cys did not destroy the crystal structure of the CQDs. To explore the effect of post-processing on the optical properties of the CQDs, we carried out UV-vis as well as PL spectra. Figure 1b shows the UV-vis and the PL of the pristine and Cys-processed CQDs. The absorption and emission peaks of pristine CQDs are located at 680 and 685 nm, which are identified as belonging to CQDs [17,33]. After Cys post-processing, the PL of the CQDs shows a slight redshift to 686–688 nm with different concentrations of Cys, which are marked in Figure 1d. Moreover, as shown in Figure 1b, both the pristine and cys-processed

CQDs show narrow PL curves, and the Cys-processed CQDs exhibit a narrower average full-width at half-maximum (FWHM) of 32 nm compared to the 36 nm FWHM of the pristine counterparts. This indicates that the size of CQDs is more homogeneous after Cys post-processing. Meanwhile, the PL intensity of the CQDs gradually varies with the concentration of Cys, and when the concentration of Cys reached 0.05 M, the PL intensity achieved the maximum (Figure 1d). Furthermore, TRPL decay tests were conducted, as shown in Figure 1c. These CQDs have an obvious biexponential decay characteristic, and the fitted parameters of PL decay curves and average lifetime (τ_{ave}) are summarized in Table 1. As shown in Figure 1d, the τ_{ave} of CQDs shows the same pattern as PL intensity with increasing Cys concentration. The CQDs with 0.05 M Cys processing have the longest τ_{ave} of 45.17 ns, which is higher than that of 31.45 ns for the pristine CQDs. These are attributed to the fact that low levels of Cys effectively suppress the surface defects of the CQDs, while, as Cys increases, the excess Cys remaining in solution provides the nucleation sites that drive the aggregation of CQDs, which leads to the aggregation and sedimentation of the active ingredients in the colloidal solution [41,42]. Meanwhile, the coordination of Cys on the surface of the CQDs changes from tridentate to bidentate as its concentration increases from low to high, which weakens the defect suppression effect [43].

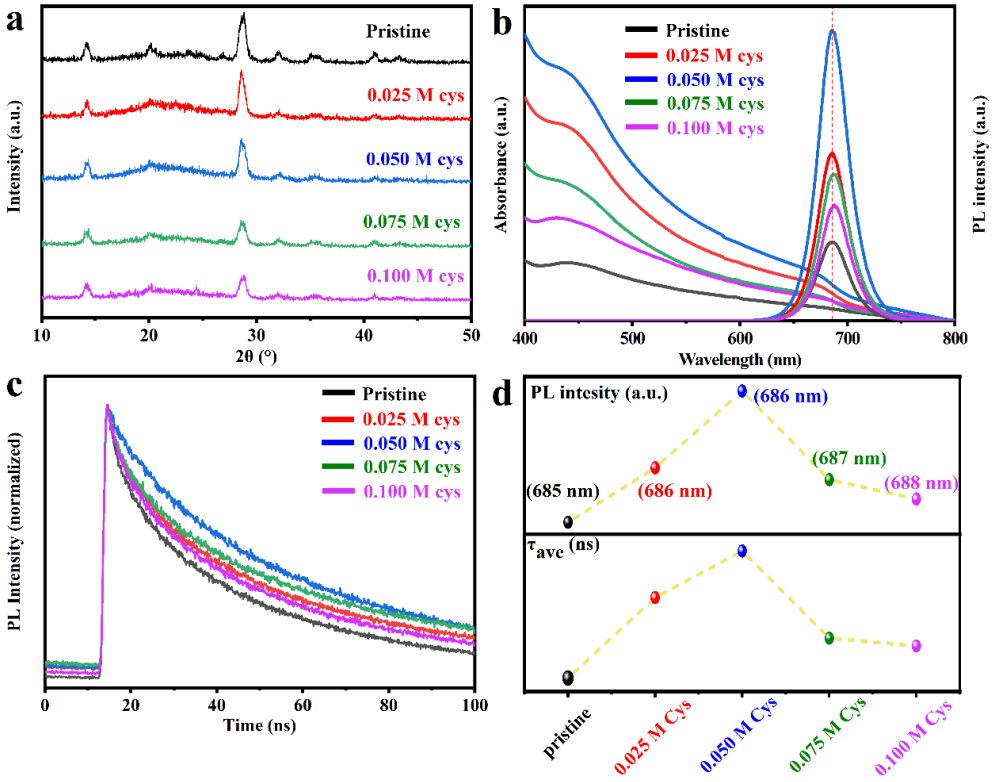

Figure 1. (**a**) XRD patterns of the pristine and Cys-processed CQDs. (**b**) UV-vis spectra and PL spectra of the pristine and Cys-processed CQDs. (**c**) Time-resolved photoluminescence (TRPL) spectra of the pristine and Cys-processed CQDs. (**d**) The trend of maximum PL peak and τ_{ave} of CQDs with different Cys content.

Table 1. Lifetime decay parameters and calculated average lifetimes of CQDs.

Samples	τ_1	τ_2	B_1	B_2	τ_{ave}
Pristine	3.84	32.67	2455.10	6521.97	31.45
0.025 M cys	4.87	41.40	1965.49	6462.34	40.14
0.050 M cys	7.32	46.11	1204.40	7724.70	45.17
0.075 M cys	4.60	37.00	2116.05	6613.22	35.76
0.100 M cys	4.26	36.14	2239.13	6621.54	34.92

Further investigations were carried out for the optimal concentration (0.050 M) of Cys-processed CQDs. The pristine CQDs capped with oleic acid and oleylamine revealed a low PLQY of 38.61%. After post-processing with the Cys-EtOAc solution, the PLQY of the CQDs increased to 70.77% (Figure 2), nearly twice as much as the pristine samples. These results show that the Cys-processed CQDs have a lower trap density and fewer surface defects. We calculated the radiative and non-radiative rates according to the following three equations:

$$\tau_r = \frac{\tau_{ave}}{PLQY} \quad (1)$$

$$k_r = \frac{1}{\tau_r} \quad (2)$$

$$k_{nr} = \frac{1}{\tau_{ave}} - k_r \quad (3)$$

where τ_r represents the radiation recombination lifetime and k_r and k_{nr} represent the radiative rate and the non-radiative rate of the CQDs, respectively. The results are shown in Table 2. The k_{nr} of the 0.050 M Cys-processed CQDs is 0.0064 ns^{-1}, which is less than that of the pristine CQDs (0.0108 ns^{-1}). Automatically, the k_r of CQDs after Cys processing is increased to 0.0157 ns^{-1} compared with that of pristine (0.0108 ns^{-1}) CQDs. This suggests that the Cys suppressed surface defects because of reducing the non-radiative recombination.

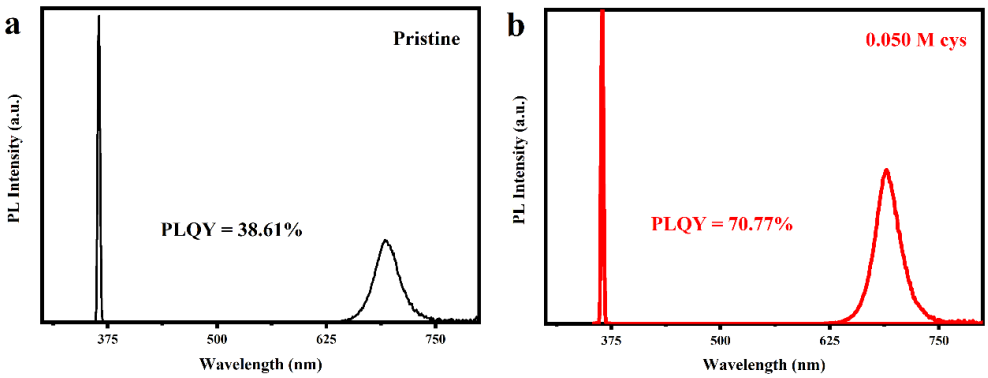

Figure 2. PLQY measurement of (**a**) the pristine and (**b**) Cys-processed CQDs.

Table 2. PLQYs and calculated kr (ns^{-1}) and knr (ns^{-1}) of the pristine and Cys-processed CQDs.

Samples	PLQY (%)	k_r (ns^{-1})	k_{nr} (ns^{-1})
Pristine	38.61	0.0108	0.0108
0.050 M cys	70.77	0.0157	0.0064

To further demonstrate that the Cys combines strongly with the perovskites, we performed the XPS of pristine and Cys-processed CQDs. As shown in Figure 3a for Pb 4f, the pristine QDs have a lower binding energy of 138.05 eV and 142.91 eV compared with that of 138.23 eV and 143.11 eV for Cys-processed QDs, suggesting that the lead ions combine with Cys for their high binding force. Figure 3b shows similar offsets in I 3d, and the peaks in the I 3d spectrum that corresponded to the $3d^{5/2}$ and $3d^{3/2}$ oxidation states of I shifted from 618.95 to 618.98 eV and 630.43 to 630.52 Ev, respectively, indicating the adjustment in the chemical bonding between Pb^{2+} and I^- owing to the incorporation of Cys. Figure 3c is the FTIR spectra of the pristine and the Cys-processed CQDs. For the pristine CQDs capped with OA and OAm, the peaks at 2850–2930 cm^{-1} originate from the stretching mode (ν(C-H)) of alkane in the OA and OAm ligands. The peak at 1711 cm^{-1} is the characteristic peak from OA (νas(coo-)). After ligand exchange with cysteine, the peaks of Cysteine ligands showed up (3166, 1646, 1270, 1055, and 753 cm^{-1}). These results proved that the Cys, as a new ligand, combined with the surface of the perovskites and had stronger coordination interaction between Pb^{2+} and Cys [33]; the post-processing of

CQDs surface defects by Cys is illustrated in Figure 3d. Diverse functional groups of Cys effectively suppress uncoordinated lead as well as iodine on the surface of CQDs.

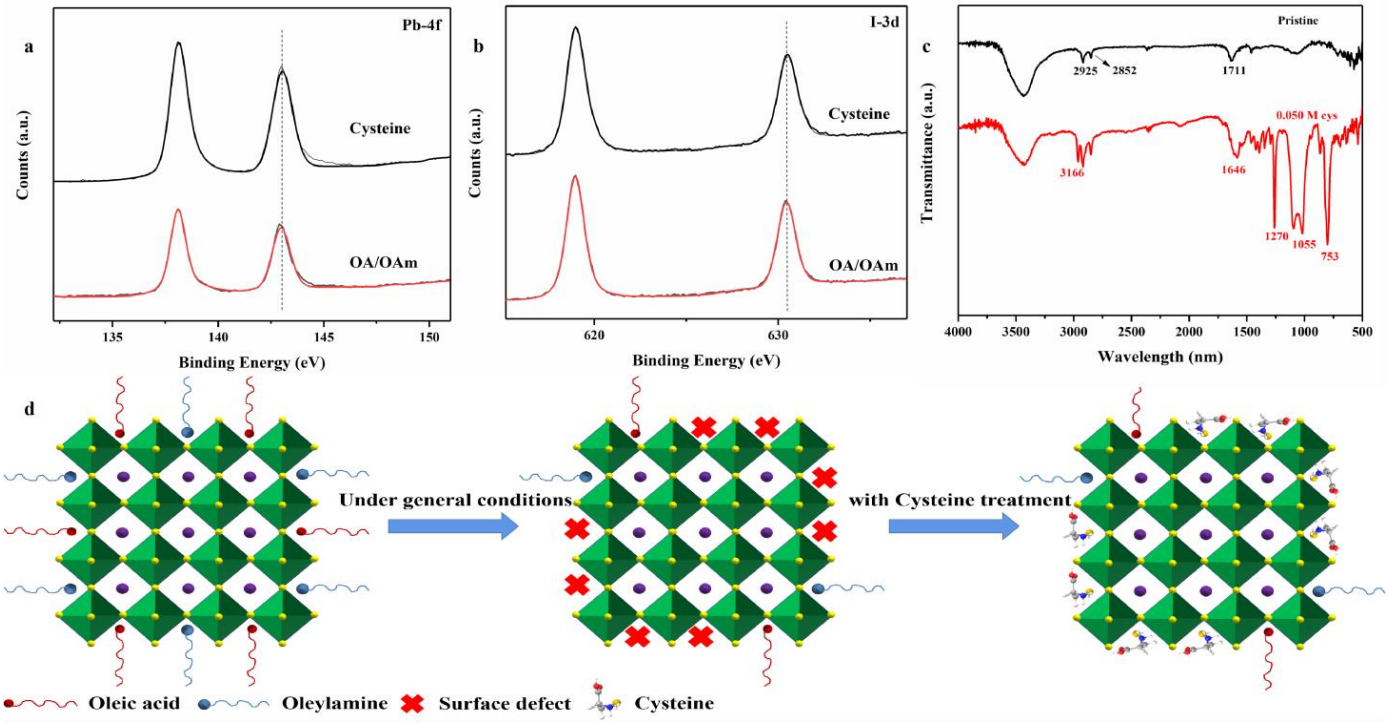

Figure 3. XPS spectra of the pristine and the Cys-processed CQDs (**a**) Pb 4f and (**b**) I 3d. (**c**) FTIR spectra of the pristine (capped with OA/OAm) and Cys-processed CQDs. (**d**) Schematic of the post-processing of CQDs by Cys.

The transmission electron microscope (TEM) was used to investigate the morphology of the QDs and observe the close-packed particle arrangement after the ligand exchange procedures. As is shown in Figure 4a,b, both the as-synthesized QDs have an obvious cubic morphology in non-polar solvents, which suggests that the lattice remains unchanged after the ligand exchange. The average particle sizes of the pristine CQDs and the Cys-processed samples are 14 and 16 nm, respectively; the corresponding size distributions are shown in Figure 4e,f. Figure 4c,d show high-resolution TEM (HR-TEM) images of single CQDs from Figure 4a,b, respectively. The well-resolved lattices indicate that the CQDs are single-crystalline CQDs. The interplanar distance of both samples is 0.31 nm, corresponding to the (100) plane of α-CQDs. The post-processing of CQDs by Cys did not affect the crystallization process of the CQDs and it remained in the cubic phase, which was consistent with the XRD, and Cys did not enter the interior of the CQDs and only acted on the surface of it.

Time-dependent XRD and the PL intensity of CQDs were used to evaluate the stability of CQDs. By comparing the phase stability of the pristine and Cys-processed CQDs in an atmosphere with an average temperature of 30 °C and an average humidity of 85%, it was found that the black α phase of pristine CQDs was almost completely converted to the optically inactive δ phase after 20 days (Figure 5a) [33]. At this point, the Cys-processed CQDs still retained the black α phase (Figure 5b). Synchronously, we measured the PL spectra of the pristine and the Cys-processed CQDs after storage under an identical atmospheric environment for a while. As is shown in Figure 5c,d, it is obvious that the Cys-processed CQDs retained more than 86% of the initial PL intensity after 20 days of storage, while the PL intensity of the original CQDs at the same conditions decreased almost to quenching. This is due to the small molecule of Cys accompanied by a small spatial site resistance. It is more effective in post-processing through the close contact of

multifunctional functional groups with the surface of CQDs while isolating water and oxygen from the atmosphere, greatly improving the stability of the CQDs [16,34].

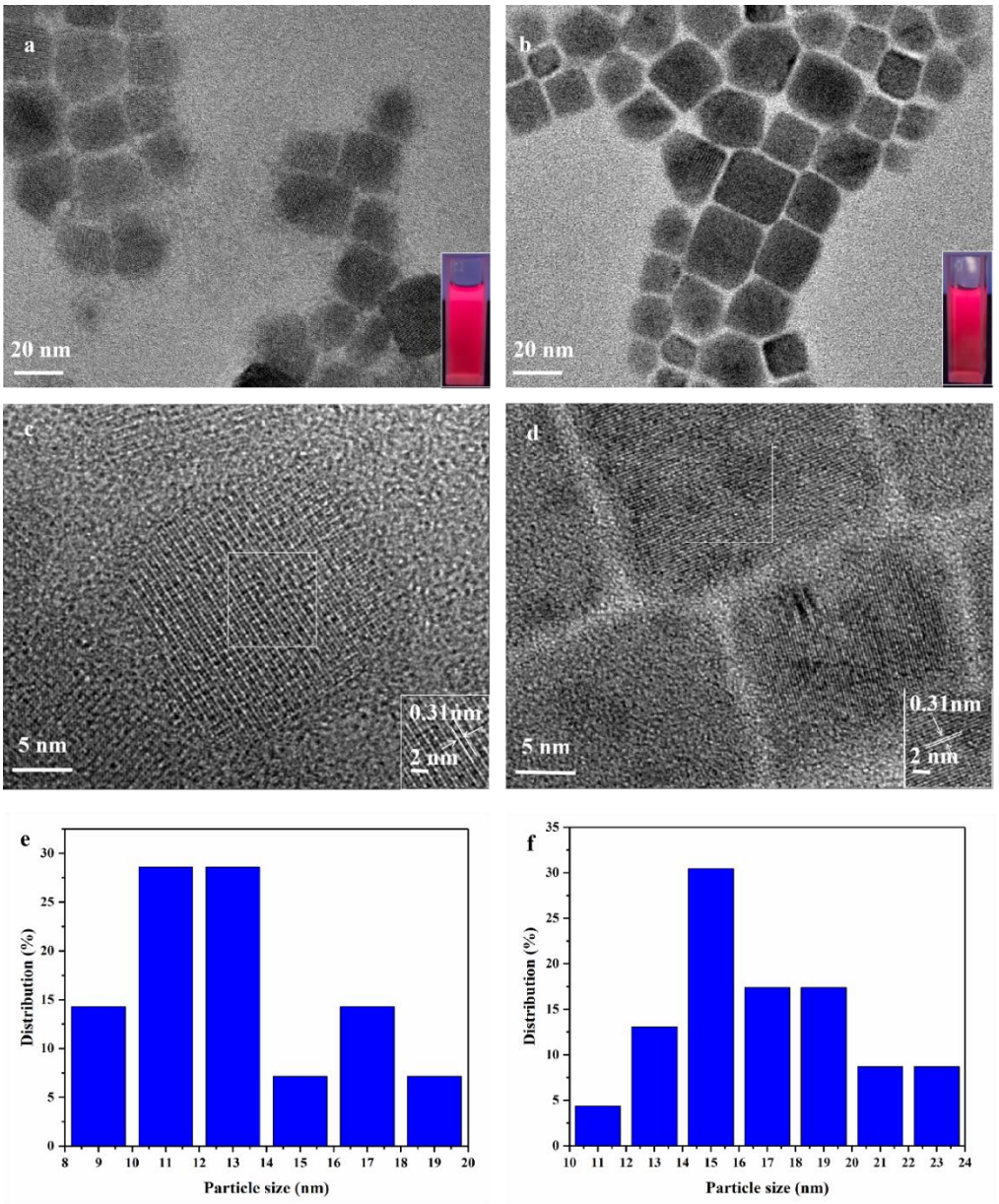

Figure 4. TEM and solution under ultraviolet illumination images of (**a**) pristine CQDs and (**b**) the Cys-processed CQDs. HR-TEM images of (**c**) the pristine CQDs and (**d**) the Cys-processed CQDs. Corresponding size distribution of (**e**) the pristine CQDs and (**f**) the Cys-processed CQDs.

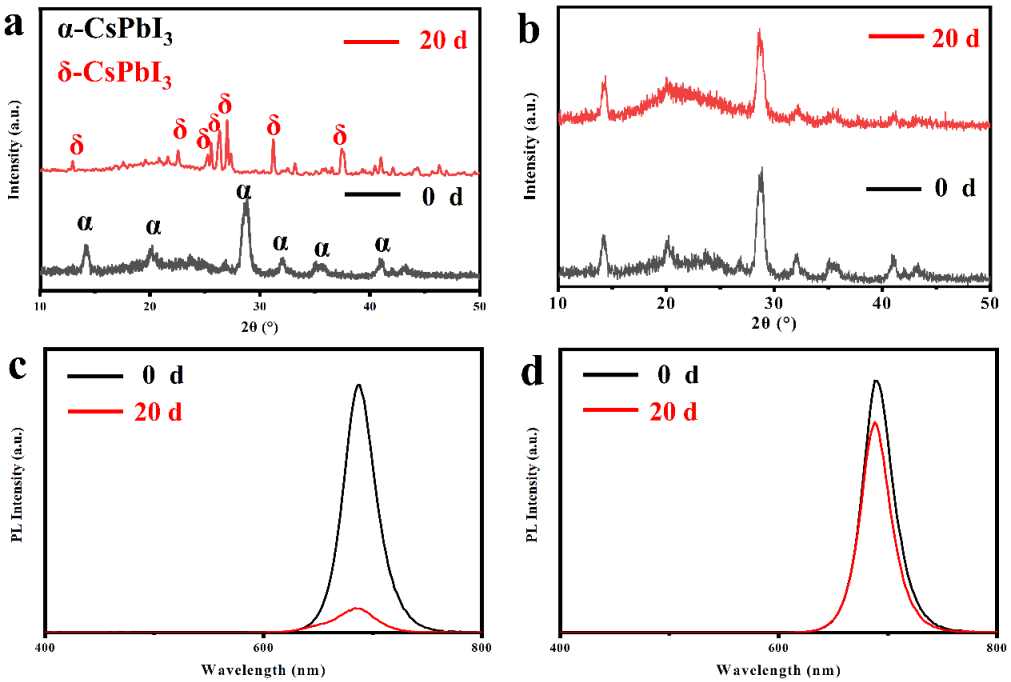

Figure 5. Time-dependent XRD of (**a**) the pristine and (**b**) the Cys-processed CQDs. Time-dependent PL spectra of (**c**) the pristine and (**d**) the Cys-processed CQDs after storage under an atmosphere with an average temperature of 30 °C and an average humidity of 85% for 20 days.

5. Conclusions

In summary, the CQDs were successfully prepared by the hot-injection method, while ligand exchange with Cys was completed in an atmosphere with an average temperature of 30 °C and an average humidity of 85%. The Cys-processed CQDs retained more than 86% of the initial PL intensity after 20 days of storage in the atmosphere environment, and the Cys also enhanced the PLQY of the CQDs. The PLQY of the Cys-processed CQDs is 70.77%, nearly twice as much as that of the pristine CQDs. This is attributed to the stronger binding force between the Cys and lead ions on the surface of perovskites. This work provides a new avenue for applications in high-performance and stable photovoltaic or other optoelectronic devices.

Author Contributions: Investigation and writing—original draft preparation, S.C.; writing—review and editing, J.W.; supervision and project administration, Q.P. All authors have read and agreed to the published version of the manuscript.

Funding: This research was funded by the National Natural Science Foundation of China grant number 21965003.

Data Availability Statement: Not applicable.

Conflicts of Interest: The authors declare no conflict of interest.

References

1. Nedelcu, G.; Protesescu, L.; Yakunin, S.; Bodnarchuk, M.I.; Grotevent, M.J.; Kovalenko, M.V. Fast Anion-Exchange in Highly Luminescent Nanocrystals of Cesium Lead Halide Perovskites ($CsPbX_3$, X = Cl, Br, I). *Nano Lett.* **2015**, *15*, 5635–5640. [CrossRef] [PubMed]
2. Rao, L.; Yong, T.; Yan, C.; Li, J.; Zhong, G.; Tang, K.; Yu, B.; Li, Z.; Zhang, J.Z. Tuning the emission spectrum of highly stable cesium lead halide perovskite nanocrystals through poly (lactic acid)—Assisted anion-exchange reactions. *J. Mater. Chem. C* **2018**, *6*, 5375–5383. [CrossRef]
3. Brown, A.A.; Damodaran, B.; Jiang, L.; Tey, J.N.; Pu, S.H.; Mathews, N.; Mhaisalkar, S.G. Lead Halide Perovskite Nanocrystals: Room Temperature Syntheses toward Commercial Viability. *Adv. Energy Mater.* **2020**, *10*, 2001349. [CrossRef]

4. Protesescu, L.; Yakunin, S.; Bodnarchuk, M.I.; Krieg, F.; Caputo, R.; Hendon, C.H.; Yang, R.X.; Walsh, A.; Kovalenko, M.V. Nanocrystals of Cesium Lead Halide Perovskites ($CsPbX_3$, X = Cl, Br, and I): Novel Optoelectronic Materials Showing Bright Emission with Wide Color Gamut. *Nano Lett.* **2015**, *15*, 3692–3696. [CrossRef]
5. Fu, P.; Shan, Q.; Shang, Y.; Song, J.; Zeng, H.; Ning, Z.; Gong, J. Perovskite nanocrystals: Synthesis, properties and applications. *Sci. Bull.* **2017**, *62*, 369–380. [CrossRef]
6. Song, J.; Li, J.; Li, X.; Xu, L.; Dong, Y.; Zeng, H. Quantum Dot Light-Emitting Diodes Based on Inorganic Perovskite Cesium Lead Halides ($CsPbX_3$). *Adv. Mater. (Deerfield Beach Fla.)* **2015**, *27*, 7162–7167. [CrossRef] [PubMed]
7. Sanehira, E.M.; Marshall, A.R.; Christians, J.A.; Harvey, S.P.; Luther, J.M. Enhanced mobility $CsPbI_3$ quantum dot arrays for record-efficiency, high-voltage photovoltaic cells. *Sci. Adv.* **2017**, *3*, eaao4204. [CrossRef] [PubMed]
8. Lin, K.; Xing, J.; Quan, L.N.; Arquer, F.P.G.D.; Gong, X.; Lu, J.; Xie, L.; Zhao, W.; Zhang, D.; Yan, C. Perovskite light-emitting diodes with external quantum efficiency exceeding 20 per cent. *Nature* **2018**, *562*, 245–248. [CrossRef]
9. Lu, M.; Guo, J.; Sun, S.; Lu, P.; Zhang, X.; Shi, Z.; Yu, W.W.; Zhang, Y. Surface ligand engineering-assisted $CsPbI_3$ quantum dots enable bright and efficient red light-emitting diodes with a top-emitting structure. *Chem. Eng. J.* **2021**, *404*, 126563. [CrossRef]
10. Xing, K.; Cao, S.; Yuan, X.; Zeng, R.; Li, H.; Zou, B.; Zhao, J. Thermal and photo stability of all inorganic lead halide perovskite nanocrystals. *Phys. Chem. Chem. Phys.* **2021**, *23*, 17113–17128. [CrossRef]
11. Leijtens, T.; Bush, K.; Cheacharoen, R.; Beal, R.; Bowring, A.; Mcgehee, M. Towards enabling stable lead halide perovskite solar cells; interplay between structural, environmental, and thermal stability. *J. Mater. Chem. A* **2017**, *5*, 11483–11500. [CrossRef]
12. Shen, X.; Wang, S.; Zhang, X.; Wang, H.; Zhang, X.; Wang, C.; Gao, Y.; Shi, Z.; Yu, W.W.; Zhang, Y. Enhancing the efficiency of $CsPbX_3$ (X = Cl, Br, I) nanocrystals via simultaneous surface peeling and surface passivation. *Nanoscale* **2019**, *11*, 11464–11469. [CrossRef] [PubMed]
13. Yao, Z.; Zhao, W.; Liu, S.F. Stability of the $CsPbI_3$ perovskite: From fundamentals to improvements. *J. Mater. Chem. A* **2021**, *9*, 11124–11144. [CrossRef]
14. Ji, Y.; Wang, M.; Yang, Z.; Qiu, H.; Gaponenko, N.V. Highly Stable Na: $CsPb(Br,I)_3$@Al_2O_3 Nanocomposites Prepared by Pre-protection Strategy. *Nanoscale* **2020**, *12*, 6403–6410. [CrossRef] [PubMed]
15. Bi, C.; Wang, S.; Wen, W.; Yuan, J.; Cao, G.; Tian, J. Room-Temperature Construction of Mixed-Halide Perovskite Quantum Dots with High Photoluminescence Quantum Yield. *J. Phys. Chem. C Nanomater. Interfaces* **2018**, *122*, 5151–5160. [CrossRef]
16. Chen, K.; Zhong, Q.; Chen, W.; Sang, B.; Wang, Y.; Yang, T.; Liu, Y.; Zhang, Y.; Zhang, H. Short-Chain Ligand-Passivated Stable α-$CsPbI_3$ Quantum Dot for All-Inorganic Perovskite Solar Cells. *Adv. Funct. Mater.* **2019**, *29*, 1900991. [CrossRef]
17. Xu, T.; Liu, B.; Liu, Z.; Li, J. Stability of $CsPbX_3$ (X=Br, Cl, I) perovskite nanocrystalline. *J. Solid State Chem.* **2022**, *316*, 123536. [CrossRef]
18. Kajal, S.; Kim, J.; Yun, S.S.; Singh, A.N.; Kim, K.S. Unfolding the Influence of Metal Doping on Properties of $CsPbI_3$ Perovskite. *Small Methods* **2020**, *4*, 2000296. [CrossRef]
19. Yao, Z.; Zhao, W.; Chen, S.; Jin, Z.; Liu, S.F. Mn Doping of $CsPbI_3$ Film Towards High-Efficiency Solar Cell. *ACS Appl. Energy Mater.* **2020**, *3*, 5190–5197. [CrossRef]
20. Shen, W.; Zhang, J.; Dong, R.; Chen, Y.; Yang, L.; Chen, S.; Su, Z.; Dai, Y.; Cao, K.; Liu, L. Stable and Efficient Red Perovskite Light-Emitting Diodes Based on Ca^{2+}-Doped $CsPbI_3$ Nanocrystals. *Research* **2021**, *2021*, 9829374. [CrossRef]
21. Chen, C.; Xuan, T.; Bai, W.; Zhou, T.; Xie, R.J. Highly Stable $CsPbI_3$:Sr^{2+} Nanocrystals with Near-Unity Quantum Yield enabling Perovskite Light-Emitting Diodes with an External Quantum Efficiency of 17.1%. *Nano Energy* **2021**, *85*, 106033. [CrossRef]
22. Wang, C.; Song, Z.; Li, C.; Zhao, D.; Yan, Y. Low-Bandgap Mixed Tin-Lead Perovskites and Their Applications in All-Perovskite Tandem Solar Cells. *Adv. Funct. Mater.* **2019**, *29*, 1808801. [CrossRef]
23. Liu, D.; Shao, Z.; Li, C.; Pang, S.; Yan, Y.; Cui, G. Structural Properties and Stability of Inorganic CsPbI3 Perovskites. *Small Struct.* **2020**, *2*, 2000089.
24. Zhang, J.; Yang, L.; Zhong, Y.; Hao, H.; Yang, M.; Liu, R. Improved phase stability of the $CsPbI_3$ perovskite via organic cation doping. *Phys. Chem. Chem. Phys.* **2019**, *21*, 11175–11180. [CrossRef]
25. Yong, W.; Zhang, T.; Feng, X.; Li, Y.; Zhao, Y. A Facile Low Temperature Fabrication of High Performance $CsPbI_2Br$ All-Inorganic Perovskite Solar Cells. *Sol. RRL* **2018**, *2*, 1700180.
26. Yao, Z.; Jin, Z.; Zhang, X.; Wang, Q.; Liu, S. Pseudohalide (SCN)-doped $CsPbI_3$ for high-performance solar cells. *J. Mater. Chem. C* **2019**, *7*, 13736–13742. [CrossRef]
27. Qi, W.; Li, J.; Li, Y.; Sohail, K.; Zhang, X. Manipulated Crystallization and Passivated Defects for Efficient Perovskite Solar Cells via Addition of Ammonium Iodide. *ACS Appl. Mater. Interfaces* **2021**, *13*, 34053–34063. [CrossRef]
28. Yao, J.S.; Ge, J.; Wang, K.H.; Zhang, G.; Zhu, B.S.; Chen, C.; Zhang, Q.; Luo, Y.; Yu, S.H.; Yao, H.B. Few-Nanometer-Sized α-$CsPbI_3$ Quantum Dots Enabled by Strontium Substitution and Iodide Passivation for Efficient Red-Light Emitting Diodes. *J. Am. Chem. Soc.* **2019**, *141*, 2069–2079. [CrossRef]
29. Lu, M.; Zhang, X.; Zhang, Y.; Guo, J.; Shen, X.; Yu, W.W.; Rogach, A.L. Simultaneous Strontium Doping and Chlorine Surface Passivation Improve Luminescence Intensity and Stability of $CsPbI_3$ Nanocrystals Enabling Efficient Light-Emitting Devices. *Adv. Mater.* **2018**, *30*, 1804691. [CrossRef]
30. Baek, S.; Kim, Y.; Kim, S.W. Highly photo-stable $CsPbI_3$ perovskite quantum dots via thiol ligand exchange and their polymer film application. *J. Ind. Eng. Chem.* **2020**, *83*, 279–284. [CrossRef]

31. Jka, B.; Bk, B.; Whk, A.; Jc, C.; Cc, A.; Sjl, D.; Jsl, C.; Dhk, A.; Min, J.; Yk, A. Alkali acetate-assisted enhanced electronic coupling in $CsPbI_3$ perovskite quantum dot solids for improved photovoltaics—ScienceDirect. *Nano Energy* **2019**, *66*, 104130.
32. Pan, J.; Shang, Y.; Yin, J.; Bastiani, M.; Wei, P.; Dursun, I.; Sinatra, L.; El-Zohry, A.M.; Hedhili, M.N.; Emwas, A.H. Bidentate Ligand-passivated $CsPbI_3$ Perovskite Nanocrystals for Stable Near-unity Photoluminescence Quantum Yield and Efficient Red Light-emitting Diodes. *J. Am. Chem. Soc.* **2017**, *140*, 562–565. [CrossRef] [PubMed]
33. Huynh, K.A.; Bae, S.-R.; Nguyen, T.V.; Do, H.H.; Heo, D.Y.; Park, J.; Lee, T.-W.; Le, Q.V.; Ahn, S.H.; Kim, S.Y. Ligand-Assisted Sulfide Surface Treatment of $CsPbI_3$ Perovskite Quantum Dots to Increase Photoluminescence and Recovery. *ACS Photonics* **2021**, *8*, 1979–1987. [CrossRef]
34. Bi, C.; Kershaw, S.V.; Rogach, A.L.; Tian, J. Improved Stability and Photodetector Performance of $CsPbI_3$ Perovskite Quantum Dots by Ligand Exchange with Aminoethanethiol. *Adv. Funct. Mater.* **2019**, *29*, 1902446. [CrossRef]
35. Shi, J.; Li, F.; Jin, Y.; Liu, C.; Ma, W. In Situ Ligand Bonding Management of $CsPbI_3$ Perovskite Quantum Dots Enables High Performance Photovoltaics and Red Light-Emitting Diodes. *Angew. Chem. Int. Ed.* **2020**, *59*, 22230–22237. [CrossRef]
36. Jia, D.; Chen, J.; Yu, M.; Liu, J.; Johansson, E.; Hagfeldt, A.; Zhang, X. Dual Passivation of $CsPbI_3$ Perovskite Nanocrystals with Amino Acid Ligands for Efficient Quantum Dot Solar Cells. *Small* **2020**, *16*, 2001772. [CrossRef]
37. Kurihara, T.; Matano, A.; Noda, Y.; Takegoshi, K. Rotational Motion of Ligand-Cysteine on CdSe Magic-Sized Clusters. *J. Phys. Chem. C* **2019**, *123*, 14993–14998. [CrossRef]
38. Kurihara, T.; Noda, Y.; Takegoshi, K. Capping Structure of Ligand-Cysteine on CdSe Magic-Sized Clusters. *ACS Omega* **2019**, *4*, 3476–3483. [CrossRef]
39. Kurihara, T.; Noda, Y.; Takegoshi, K. Quantitative Solid-State NMR Study on Ligand-Surface Interaction in Cysteine-Capped CdSe Magic-Sized Clusters. *J. Phys. Chem. Lett.* **2017**, *8*, 2555–2559. [CrossRef]
40. Cui, Y.; Lou, Z.; Wang, X.; Yu, S.; Yang, M. A study of optical absorption of cysteine-capped CdSe nanoclusters using first-principles calculations. *Phys. Chem. Chem. Phys.* **2015**, *17*, 9222–9230. [CrossRef]
41. Pan, A.; He, B.; Fan, X.; Liu, Z.; Urban, J.J.; Alivisatos, A.P.; He, L.; Liu, Y. Insight into the Ligand-Mediated Synthesis of Colloidal $CsPbBr_3$ Perovskite Nanocrystals: The Role of Organic Acid, Base, and Cesium Precursors. *ACS Nano* **2016**, *10*, 7943–7954. [CrossRef] [PubMed]
42. Zhang, X.; Huang, H.; Maung, Y.M.; Yuan, J.; Ma, W. Aromatic amine-assisted pseudo-solution-phase ligand exchange in $CsPbI_{(3)}$ perovskite quantum dot solar cells. *Chem. Commun. (Camb)* **2021**, *57*, 7906–7909. [CrossRef] [PubMed]
43. Kuznetsova, V.A.; Mates-Torres, E.; Prochukhan, N.; Marcastel, M.; Purcell-Milton, F.; O'Brien, J.; Visheratina, A.K.; Martinez-Carmona, M.; Gromova, Y.; Garcia-Melchor, M.; et al. Effect of Chiral Ligand Concentration and Binding Mode on Chiroptical Activity of CdSe/CdS Quantum Dots. *ACS Nano* **2019**, *13*, 13560–13572. [CrossRef] [PubMed]

Disclaimer/Publisher's Note: The statements, opinions and data contained in all publications are solely those of the individual author(s) and contributor(s) and not of MDPI and/or the editor(s). MDPI and/or the editor(s) disclaim responsibility for any injury to people or property resulting from any ideas, methods, instructions or products referred to in the content.